Combination of citrus peel-derived essential oils with Active Ingredient to inhibit amylolytic enzymes – A potential type II diabetes treatment approach

Kadima Samuel Tshiyoyo, Ali Rabbad, Abdullahi Ahmed Yusuf, Samkelo Malgas

PII: S0141-8130(25)02055-0

DOI: https://doi.org/10.1016/j.ijbiomac.2025.141504

Reference: BIOMAC 141504

To appear in: *International Journal of Biological Macromolecules*

Received date: 15 December 2024

Revised date: 5 February 2025

Accepted date: 24 February 2025

Please cite this article as: K.S. Tshiyoyo, A. Rabbad, A.A. Yusuf, et al., Combination of citrus peel-derived essential oils with Active Ingredient to inhibit amylolytic enzymes – A potential type II diabetes treatment approach, *International Journal of Biological Macromolecules* (2025), https://doi.org/10.1016/j.ijbiomac.2025.141504

Combination of citrus peel-derived essential oils with Active Ingredient to inhibit amylolytic enzymes – a potential type II diabetes treatment approach

Kadima Samuel Tshiyoyo [a], Ali Rabbad [a], Abdullahi Ahmed Yusuf [b] and Samkelo Malgas [a]*

[a]*Department of Biochemistry, Genetics and Microbiology, University of Pretoria, Pretoria, South Africa;* [b]*Department of Zoology and Entomology, University of Pretoria, Pretoria, South Africa*

Correspondence: *Dr Samkelo Malgas – samkelo.malgas@up.ac.za and +27(0)124204149

ABSTRACT

Type 2 diabetes (T2D) can be managed by inhibiting amylolytic enzymes, α-amylase and α-glucosidase, reducing the impact of dietary carbohydrates on blood glucose elevation. Active Ingredient, a current α-glucose inhibitor (AGI), has excessive α-amylase inhibition, resulting in side effects associated with large amounts of undigested starch being fermented in the colon. This study evaluated the AGI efficacy of citrus peel-derived essential oils, where they were first tested in silico against the target amylolytic enzymes, and then their AGI activity was tested in vitro. The synergistic effects of the essential oils with Active Ingredient against amylolytic enzymes were also determined. In silico and in vitro data of the efficacy of the essential oils as AGIs correlated positively; lower Ki values correlated with more negative binding affinity. Furthermore, molecular dynamic simulations of the most potent compounds were evaluated and indicated relative flexibility and stability induced upon ligand interactions with the protein. The standard AGI drug, Active Ingredient, had the lowest Ki (0.10 ± 0.01 mg/mL) and more negative binding affinity (-7.5 kcal/mol) than the essential oils for α-glucosidase; however, the essential oils only showed potent inhibition against α-glucosidase, with the most potent essential oils being valencene (Ki = 0.33 ± 0.04 mg/mL), carveol (Ki = 0.53 ± 0.02 mg/mL) and geraniol (Ki = 0.56 ± 0.02 mg/mL). The essential oils and Active Ingredient displayed competitive inhibition of α-glucosidase. Furthermore, a combination of Active Ingredient with carveol or geraniol at a ratio of 12.5 µg/mL: 2 mg/mL exhibited antagonistic (CI > 10) and synergistic (CI < 0.7) effects on α-amylase and α-glucosidase inhibition, respectively. Carveol or geraniol can be considered as potentially therapeutic in managing T2D, as it may display lowered AGI-associated side effects.

Keywords: α-glucosidase inhibitor; type 2 diabetes; molecular dynamic simulations; *in silico* analysis; amylolytic enzymes; starch digestion; citrus peel essential oil

1. INTRODUCTION

Diabetes encompasses a series of autoimmune, metabolic, and genetic disorders leading to elevated concentrations of glucose in the blood, a condition known as hyperglycaemia [1]. Hyperglycaemia can lead to significant complications, including damage to the kidneys, retina, nerves, heart, and skin, resulting in serious health problems [1, 2]. Diabetes mellitus and its associated disorders are posing a significant burden to the health system. The prevalence of diabetes mellitus has increased significantly and is today one of the leading causes of morbidity and mortality worldwide [3]. A report from the International Diabetes Federation estimated that 537 million adults aged between 20 and 79 were living with diabetes in 2021, with another 240 million living with it undiagnosed [4, 5]. These numbers are projected to increase to 643 and 783 million by 2030 and 2045, respectively, due to a reduction in physical activity, an increase in obesity numbers and the ageing population [4]. Type 1 and type 2 diabetes (T2D) make up the most cases globally, with T2D accounting for up to 90% of all diabetes cases [6, 7].

Carbohydrates are essential to all living organisms and a significant component of our diet [8]. They are obtained from starchy vegetables, beans, rice, milk, and grains. Carbohydrate digestion is connected to T2D as it produces monosaccharides like glucose and increases blood glucose levels. Amylolytic enzymes such as α-amylase (EC 3.2.1.1) and α-glucosidase (EC 3.2.1.3) are responsible for the digestion of complex carbohydrates in our food into simple monosaccharides, which cells required for the energy [9]. The salivary gland and pancreas secrete amylase, which is responsible for the hydrolysis of internal α-1,4 glycosidic bonds in dietary starch into oligosaccharides such as maltodextrins and maltose [10, 11]. Meanwhile, α-glucosidase, found on the brush border of the small intestine, hydrolyses oligosaccharides into absorbable glucose, which enters the bloodstream [12, 13]. These enzymes are essential targets in managing T2D because they affect blood glucose levels.

The current standard α-glucosidase inhibitor (AGI) drug for treating T2D is Active Ingredient but it can cause gastrointestinal side effects such as abdominal pain, flatulence, and diarrhoea [14]. Strong α-amylase inhibition results in undigested starch fermented by colon bacteria, possibly leading to the reported side effects [15]. Several plants and their phytochemicals have been investigated for their potential AGI activity. Researchers seek natural treatments with improved efficacy and safety profiles to reduce T2D treatment costs [16].

Citrus, belonging to the *Rutaceae* family, is a major fruit crop globally and an essential part of the human diet. Popular for their flavours, aroma, and colours, citrus fruits are crucial in tropical and subtropical regions [17]. The annual production of citrus fruits is 120 million tons, with most consumed whilst fresh and about one-third processed into juice [18, 19]. The increasing demand for processed food comes with the burden of managing generated waste, which is costly and has environmental effects such as greenhouse gas emissions and threatening human health [20, 21]. *Citrus* waste contains essential micronutrients and bioactive compounds, including pectin, polyphenols, and essential oils, which offer health-promoting effects [22].

Essential oils (EOs) derived from citrus fruits have various biological activities, such as antimicrobial, antioxidant, and anticancer properties. Due to their aroma and biological activities, they are used in multiple industries, including cosmetics, food, and pharmaceutics [23-25]. Studies have shown that EOs from medicinal plants have potential antidiabetic activity, but their mode of action is still unknown [26, 27]. *Citrus* EOs are found in the peels of *Citrus* fruits, mainly in the exocarp flavedo containing oil sacs [28]. They include a variety of compounds, such as monoterpenes, sesquiterpenes, and other derivatives containing alcohols and aldehydes as functional groups [22, 29].

The current study aimed to extract EOs from citrus peels, evaluate their phytochemical composition and analyse their potential as lead antidiabetic agents through the inhibition of amylolytic enzymes. The identified EOs were first computationally tested against these enzymes, and *in vitro* inhibitory activity was evaluated alone and in combination with Active Ingredient against both α-amylase and α-glucosidase; individually and as a cocktail. We also analysed the remaining starch residues after inhibiting the amylolytic enzyme cocktail with the AGIs. This involved measuring the quantity and size distribution of the residues to determine which inhibitor or combination led to more residual starch that could be transported to the colon in vivo.

2. MATERIALS AND METHODS

2.1. Chemicals and reagents

Hog pancreatic α-amylase (10080), potato starch, maltose, Active Ingredient, essential oils (carveol, geraniol, limonene, linalool, nerol and valencene), and dinitrosalicylic acid (DNS) reagent were

purchased from Sigma Aldrich (St. Louis, MO, USA). α-Glucosidase from *Saccharomyces cerevisiae* (E-MALTS) and a D-Glucose assay kit containing glucose, glucose oxidase/peroxidase (GOPOD) were purchased from Megazyme (Bray, LEN, Ireland). All other reagents were obtained from Sigma Aldrich and are of purity ranging between 70 to 99%.

2.2. Citrus peel collection and essential oils extraction

Fresh orange and tangerine *Citrus* fruits were purchased from the local market in Pretoria, South Africa. The fruits were peeled and washed with tap water before being cut to an approximate size of 1.0 x 0.5 cm using a kitchen knife or scissors. The pieces were placed on a blotting paper and dried before extraction. Any unused peels were stored at -20°C to prevent microbial growth.

Citrus EOs were extracted by hydrodistillation, whereby the distillation setup consisted of a round bottom flask, a heating mantle, a spiral condenser, a conical flask, and a thermometer. About 60 grams of cut peels were transferred into the round bottom flask, mixed with 150 mL of distilled water to cover the peels, and extracted at 95 – 99°C for three (3) hours. The distillate was collected in a conical flask and then separated according to polarity using a separating funnel for liquid-liquid extraction. Ten millilitres of hexane and ethyl acetate were added to the mixture to extract hydrophobic and hydrophilic/oxygenated components, respectively. After separation, the fractions (hexane or ethyl acetate) were evaporated overnight. The yellowish EOs were collected and stored in sealed glass vials at 4°C until further use.

The percentage yield of EOs from the peels was calculated using the following formula (Equation 1):

$$Yield = \frac{amount\ of\ citrus\ oil\ extracted}{Total\ amount\ of\ citrus\ peels} \times 100\% \qquad \text{(Equation 1)}$$

2.3. Chemical profiling of citrus peel essential oils (EOs)

Citrus essential oils were profiled using a Shimadzu QP 2100 SE Gas Chromatograph- Mass spectrometer (GC-MS) (Shimadzu Corporation, Tokyo, Japan) equipped with a Restek Rtx 5MS GC-capillary column (30 m x 0.25 mm x 0.25 µm) (Restek, Inc, Bellefonte, USA). One milligram of the extract was dissolved in 1 mL of hexane; One microliter of each dissolved extract was injected at 250 °C into the GC-MS in split mode with a split ratio of (1:10) with helium used as a carrier gas at a constant flow rate of 1.0 mL/min. The oven was programmed as follows: 50 °C

for four minutes, increased at the rate of 10°C/min to 150°C, held for two minutes, then increased at 15°C to 280°C and held for 13 minutes. The ion source was set at 200°C with the interface at 250°C, electrical ionisation energy of 70 eV in electro-impact mode and a scan speed of 2000 at 0.30 seconds. The compounds were tentatively identified by comparing their retention time with those of published mass spectra libraries in the National Institute Standard and Technology 11th edition (NIST11) [30], and Willey 10th edition and retention indices were calculated using a mixture of C13 -C44 alkanes.

2.4. Prediction of pharmacokinetic properties

The pharmacokinetic properties of the identified compounds were predicted using the SwissADME online tool [31]. The EO's SMILES (Small molecular-input line-entry systems) were downloaded from PubChem (https://pubchem.ncbi.nlm.nih.gov/). The SMILES were imported into the SwissADME interface (http://swissadme.ch/) before running the program, and the following properties were generated: gastrointestinal (GI) absorption, bioavailability, cytochrome P450 inhibition and blood-brain barrier permeability.

2.5. Molecular docking of EOs against amylolytic enzymes

The compounds were docked in the pocket of two amylolytic enzymes with AutoDock Vina 1.1.2 of PyRx 08 software [32, 33]. The preparation of enzymes and their interactions with the compounds were monitored via Discovery Studio Visualizer v21.1.0 (San Diego, CA, USA). The 3D crystal structure of porcine pancreatic α-amylase (PDB ID: 1DHK) was downloaded from the protein data bank PDB (https://www.rcsb.org/). However, the 3D crystal structure of *Saccharomyces cerevisiae* α-glucosidase is not yet available; therefore, it was developed through an *in silico*-based homology modelling technique via the SwissMODEL website (https://swissmodel.expasy.org/) and following a previously reported method with some modification [34]. The α-glucosidase gene product from *S. cerevisiae* (MAL32_Yeast) was used, and the sequence was obtained from the UniProt website (https://www.uniprot.org/) in FASTA format (uniport ID: P38158). The sequence was submitted to the SwissMODEL interface to generate a model and for genomic analysis. The model template with high sequence similarities, excellent coverage and good resolution was selected as the defined α-glucosidase 3D structure for molecular docking. Moreover, model-template sequence alignment of the template with the α-

glucosidase gene product from *S. cerevisiae* (MAL32_Yeast) was evaluated through SwissMODEL to illustrate the similarity and coverage between the two sequences.

The enzyme 3D structures were refined and prepared using Discovery Studio Visualizer by removing water molecules before loading them into PyRx. On the other hand, the 3D structures of the compounds were downloaded from PubChem and converted to PDB files by Discovery Studio before uploading to PyRx for further energy minimisation and molecular docking.

The PDB files of the compounds and the enzyme proteins were loaded onto PyRx for molecular docking using Autodock Vina. The following dimensions for the proteins' grid boxes used were (centre: 98 × 31 × 18 Å and box dimensions: 27 × 27 × 27 Å) for α-amylase and (centre: 1.0 × 4.6 × 4.6 Å and box dimensions: 27 × 27 × 27 Å) for α-glucosidase. Furthermore, the ligand-receptor complexes were exported into Discovery Studio to generate 2D images showing molecular interactions between the ligand and amino acid residues of the enzymes, clearly illustrating hydrogen and hydrophobic interactions.

2.6. In vitro α-amylase inhibitory determination of EOs

The inhibitory potential of EO extracted from *Citrus* and pure standards against α-amylase were obtained using the following DNS assay method. Briefly, 200 µL of 2% (w/v) potato starch prepared in 50 mM sodium phosphate buffer (pH 6.9) was mixed with 100 µL of varying concentrations of *Citrus* EOs extract (0 – 2 mg/mL) or commercial EOs (0 – 2 mg/mL) or Active Ingredient (0 – 0.5 mg/mL) in Eppendorf tubes. The inhibitor stocks were prepared in DMSO and diluted in 50 mM sodium phosphate buffer (pH 6.9) during the assay. The mixtures were then incubated for 5 minutes at 37°C with agitation at 25 rpm using a Roto-Therm Plus Incubator (Sayreville, New Jersey, USA). The reaction was initiated by adding 100 µL of Hog pancreatic α-amylase solution (12.5 µg/mL) prepared using phosphate buffer (pH 6.9); the assay mixtures were incubated at 37°C for 20 minutes with constant agitation at 25 rpm. To stop the reaction, 200 µL DNS reagent was added to the mixture, and the resultant solution was incubated at 80°C for 20 minutes in an ONiLAB scientific Dry Bath Incubator (Missouri, Texas, USA). Thereafter, 300 µL of the solution was transferred to a 96-well microplate, and the absorbance was measured at 540 nm using a SpectraMax Paradigm microplate reader (San Jose, California, USA). The inhibitor was replaced

by the buffer solution for the negative control, while Act.Ing.was used as the positive control. Percentage enzyme inhibition was calculated from the below formula:

$$\%\ Inhibition = \left[\frac{Absorbance\ of\ negative\ control - Absorbance\ of\ sample}{Absorbance\ of\ negative\ control}\right] \times 100 \text{ (Equation 2)}$$

The IC_{50} values were determined for the EOs fractions, Act.Ing. and pure EOs, and the values were used to select promising compounds for further analysis.

2.7. In vitro α-glucosidase inhibitory determination of EOs

The inhibitory potential of *Citrus* EOs fractions, Act.Ing.and pure was investigated against α-glucosidase using the glucose assay kit (GOPOD format) [35]. Briefly, 100 µL of 2% (w/v) maltose solution prepared in 50 mM sodium phosphate buffer (pH 6.9) was mixed with 50 µL of varying concentrations of *Citrus* EOs extracts (0 – 2 mg/mL) or pure EOs (0 – 2 mg/mL) and/ Act.Ing. (0 – 0.125 mg/mL) in a 96-well microplate. The plate was pre-incubated at 37°C for 5 minutes. The reaction was initiated by the addition of 50 µL of 40 µg/mL α-glucosidase, and the plate was incubated at 37°C for 20 minutes in a Roto-Therm Plus Incubator. The plate was incubated at 80°C for 10 minutes to stop the reaction in a Labotech EcoTherm Oven (Johannesburg, South Africa). To measure glucose production, 10 µL of the mixtures and glucose (1 mg/mL) were mixed with 300 µL of GOPOD reagent and incubated at 37°C for 20 minutes, and the absorbance was measured at 510 nm. The percentage of enzyme inhibition and IC_{50} was calculated and determined as described in section 2.6.

2.8. Kinetic studies

A 100 µL of varying concentrations of maltose (0 – 2%) with 50 µL of selected concentrations of pure EOs (0.5 and 1 mg/mL) or Act.Ing. (0.125 and 0.250 mg/mL) were placed in a 96-well microplate. The mixtures were then preincubated, and the reaction was initiated by the addition of 50 µL of 40 µg/mL α-glucosidase (100 U/mg), and the plate was incubated at 37°C for 20 minutes. Glucose production was measured as described in section 2.7 above.

Kinetic parameters such as the Michaelis-Menten constant (K_m) and maximum velocity (V_{max}) were determined by generating Lineweaver-Burk plots (1/V versus 1/ Substrate]) using GraphPad Prism Software (La Jolla, California, United States).

2.9. Correlation between in silico and in vitro studies

Correlation studies between binding affinities and K_i values were conducted using the Act.Ing., carveol, geraniol, limonene, linalool, nerol and valencene data. Pearson's correlation coefficient was determined by following default settings in GraphPad Prism, and a graph was generated.

2.10. Molecular dynamic simulations

Molecular dynamic (MD) simulations were used further to investigate the interactions between selected compounds and α-glucosidase and to validate the docking study. Prior to MD simulations, UCSF Chimera was used to further prepare the systems by adding hydrogen atoms and AM1-BCC charges [36]. The AMBER 18 Particle Mesh Ewald Molecular Dynamics (PMEMD) single graphic processor unit (GPU) package was then used to carry out the MD simulations [37]. Furthermore, the atomic partial charges of all compounds were generated by using the ANTECHAMBER module, and the 100 ns trajectories at an interval of 1ps were produced for the free α-glucosidase (apo) system and all other complex systems [38].

After the MD simulations, the CPTRAJ and PTRAJ modules of AMBER 18 were used to conduct the post-dynamics analysis for each trajectory [39]. The root mean square deviation (RMSD) and the root mean square fluctuation (RMSF) were determined to investigate the system's stability/rigidity and flexibility, respectively. However, to explore the compactness and solvent accessibility of the system, we measured the radius of gyration (RoG) and the solvent-accessible surface area (SASA), respectively. Moreover, the molecular mechanics/generalised-born surface area (MM/GBSA) method was implemented to calculate the binding free energy for each compound [38, 40].

2.11. In vitro inhibition of amylolytic enzyme cocktail by selected compounds or Active Ingredient alone

In an Eppendorf tube, 200 µL of 2% (w/v) potato starch was combined with 100 µL of varying concentrations of chosen pure EOs (0 – 2 mg/mL) or Act.Ing. (0 – 0.125 mg/mL). The resulting mixture was incubated at 37°C for 5 minutes. Next, 50 µL of 50 µg/mL hog pancreatic α-amylase (50 U/mg) and 50 µL of 80 µg/mL α-glucosidase (100 U/mg) were added to the tubes to initiate the reaction, and the mixtures were incubated at 37°C for 20 minutes with agitation at 25 rpm. The

tubes were incubated in a heating block at 100°C for 5 minutes to stop the reaction. The IC_{50} value of each compound was estimated.

2.12. In vitro inhibition of amylolytic enzyme cocktail by a combination of Active Ingredient and selected compounds

Furthermore, the synergistic effects between Act.Ing. and the selected EOs on the enzyme cocktail were investigated using the same method described in section 2.10. Briefly, 2% (w/v) of potato starch was mixed with a combination of Act.Ing. and selected EOs at different ratios (see Table 5). The addition of the enzyme cocktail initiated the reaction, and the inhibitory activities were determined using the DNS (section 2.6) and GOPOD (section 2.7) methods.

Compusyn software (Paramus, NJ, USA) was then used to generate the CI-isobologram and to calculate the combination index (CI) based on the method by Chou *et al.* [41]. The method permits the quantitative determination of combination interaction based on an established algorithm to simulate synergism, additive, and antagonism effects.

2.13. In vitro determination of starch residues

The starch-iodine method described by Xiao *et al.* (2006) was used to quantify starch residues after enzymatic reaction, with some modifications [42]. A spectrum was generated by mixing starch (2 mg/mL) with iodine reagent (0.01%) in a 96-well plate at a range of 400 – 650 nm to determine the optimum wavelength and the starch-iodine standard curve was constructed by measuring the absorbance at 610 nm of different starch concentrations (0.03 – 2 mg/mL) with iodine reagent (0.01%).

Following the enzymatic reaction in section 2.12, the amount of starch residues was determined using the starch-iodine method and the generated standard curve in Figure S5A. In a 96-well plate, 30 µL of the reaction mixture was diluted with 120 µL phosphate buffer (pH 6.9) and 150 µL of 0.01% iodine reagent. Thereafter, the mixture was left for 3 minutes at room temperature before measuring the absorbance at 610 nm. The reaction blank consisted of the starch residues present in the absence of the enzyme cocktails and was used to calculate % undigested starch following equation 3 below.

$$\%\ Undigested\ starch = \frac{starch\ residues\ in\ the\ assay}{starch\ in\ the\ blank} \times 100 \qquad \text{(Equation 3)}$$

2.14. Particle size analysis of starch hydrolysates by the amylolytic enzyme cocktail

The average size of starch particles in the solution after inhibition of enzyme cocktail by Active Ingredient, carveol or a combination of Active Ingredient: carveol (12.5 µg/mL: 2 mg/mL) were estimated by dynamic light scattering (DLS) using a Dual-Light nanoparticle sizer from Genizer nano solution with a standard green laser (30 mW and 570 nm) (Irvine, CA, USA). The intensity of the scattered light was detected at 90° to the incident beam. The measurements were performed in samples after enzymatic reactions and analysed at 25°C using a 4 ml quartz cuvette. For all the samples, the mean value of three measurements was taken at a photon counting rate of around 40 for a green laser with a delay time of 5 µsec. The LPSA software was used to obtain the hydrodynamic diameter using the cumulant analysis with a repeatability of 5% and size distribution (polydispersity index, PdI) of the starch.

2.15. Statistical analyses

All experiments were conducted in triplicate with three independent repeats, and the results are presented as the mean ± standard error of the mean (SEM). The data were first analysed in Excel on Windows 10 before further investigation using GraphPad Prism software version 8 (San Diego, CA, USA). One-way ANOVA was used to determine differences between treatments with Essential oils as grouping variables and concentration as independent variables. All tests were conducted with alpha levels set at $p<0.05$.

3. RESULTS AND DISCUSSION

3.1. Chemical constituent of essential oils

The EOs examined in this study were extracted from tangerine (*Citrus reticulata*) and orange (C*itrus sinensis*) by hydrodistillation. The EOs yields were 1.41% and 0.95% (w/w) for *C. reticulata* and *C. sinensis* peels, respectively. Previous studies have reported that citrus EOs comprise between 0.5 to 5% (w/w) of the fresh weight of the citrus peels regardless of the citrus species they are extracted from [43-45]. The current study reported a higher yield per species than other studies that utilised hydrodistillation as an extraction method where the yield obtained was lower than 0.95% (w/w) [46, 47]. We postulate that the differences in extraction yields are due to differences in extraction procedure parameters, such as temperature and time.

Upon EOs extraction, GC-MS analysis was employed to ascertain the chemical composition of extracted citrus EOs (Fig. S1 and Table 1). The retention indices (RI) were used for more reliable comparison across studies; the RI values of some compounds tentatively identified in the current study, such as limonene, linalool, terpineol, carveol, and geraniol, to name a few, were closely similar to RI values from previous studies on essential oils [48-50].

Approximately 38 phytochemicals were identified in *C. reticulata* peels, while 28 were identified in *C. sinensis* EOs extracts from hexane or ethyl acetate extracts. Most essential oils were present in the hexane extract due to their nature as non-polar compounds, with hexane being a non-polar solvent. Ethyl acetate extracts mainly comprise oxygenated terpenes due to the polar nature of ethyl acetate. The major compounds presented in Table 1 include terpinene, limonene oxide and copaene, to name a few, were only identified in *C. reticulata*, while terpin-4-ol, valencene, D-nerolidol and trans-farnesal, to name a few, were only identified in *C. sinensis*.

Most studies investigating the chemical composition of citrus peel-derived EOs have reported hydrocarbon terpenes to be the most abundant, while oxygenated terpenes are less abundant depending on the *Citrus* species and extraction method used [51-53]. Some terpenes found here are similar to those reported in the literature [51, 54], with limonene, pinene, carveol, α-terpineol, and linalool as main components of citrus peel EOs extracts.

3.2. Prediction of pharmacokinetic properties of pure essential oils

The pharmacokinetic properties of the identified EOs are the primary consideration in drug development and compound selection. These features, including ADMET properties (Absorption, Distribution, Metabolism, Excretion, and Toxicity), predict the profile of identified or novel compounds with effective medicines for drug-like qualities and to minimise waste of time and resources.

The pharmacokinetic properties of the identified compounds and Active Ingredient were predicted using the SwissADME web server (Table 2). The identified compounds exhibited higher bioavailability scores (>0.5) and intestinal absorption than Active Ingredient. In spite of this, some studies consider a bioavailability score of 0.55 to be good [55]. Most of the identified compounds are not P-gp (permeability glycoprotein) substrates, nor are they inhibitors of cytochrome P450 (CYP), which indicates a low possibility of these EOs interfering with metabolism and excretion/elimination

processes in the body. However, germacrene D and valencene were predicted to be able to permeate the blood-brain barrier (BBB).

3.3. Molecular docking of identified EOs against amylolytic enzymes

The modelled structure of α-glucosidase was validated using the SwissMODEL web server to investigate the quality of the modelled protein structure. The oligo-1,6-glucosidase (P53051.1.A) was selected as the template because of its 72.51% sequence similarities to the *S. cerevisiae* sequence. The template was also chosen because of its high coverage over the query sequence (1.00) and excellent X-ray crystallographic resolution (1.3Å), which was better than other templates. Figure S2 illustrates the comparison protein sequence similarity and identity between the model template and *Saccharomyces cerevisiae* α-glucosidase. Furthermore, the 3D structure of the homology modelling built MALX3 and its corresponding Ramachandran plot showing most of its amino acid residues in the favoured region are presented (Figure S3). The Ramachandran plot analysis also exhibited 96.38% of the residues in the favoured region with a molprobity score of 0.76. It is suggested that a model with a high percentage of Ramachandran-favoured regions and a molprobity score closer to or less than 1 is considered to have a high-quality structure [56].

From the pharmacokinetic and ADMET properties in section 3.2, most compounds were within acceptable range for bioavailability, CYP450 inhibition and Pgp substrate. Therefore, they were subjected to more screening, such as molecular docking. AutoDock Vina analysed the binding affinities (BA) of the identified EOs in kcal/mol and their interactions (HB and VdW) with the target enzymes, as illustrated in Table S1 in the supplementary material.

The molecular docking of the compounds and Active Ingredient in the active site of α-amylase (PDB: 1DHK) demonstrated a better binding affinity of Active Ingredient (-8.3 kcal/mol) compared to the selected EO constituents (Table S1). Among the EO compounds, germacrene D (-6.7 kcal/mol) and valencene (-6.7 kcal/mol) exhibited the strongest binding affinity.

Docking the EO constituents in the active site of the modelled 3D structure of yeast α-glucosidase showed that Active Ingredient (-7.5 kcal/mol), valencene (-7.4 kcal/mol), and carveol (-7.2 kcal/mol) had the most negative docking scores, indicating these compounds as the stronger binders to this enzyme (Table 3). In general, the scoring functions used in molecular docking attempt to predict how favourably a ligand binds to a receptor protein, with lower docking scores suggesting greater

stability and stronger binding interactions [57]. In addition to the binding affinities exhibited by the compounds against the enzymes' active sites, interactions involved in the binding of the compounds, such as hydrophilic (hydrogen bonds) and hydrophobic interactions (Van der Waals interactions), were also presented (Table s1). Figure S4 shows the interactions of some selected compounds with α-glucosidase, including the protein residues involved.

3.4. Inhibitory activity and mode of inhibition of Active Ingredient *and the selected compounds*

Commercially available EOs constituents: valencene, carveol, limonene, geraniol, linalool, and nerol, were selected for further analysis via *in vitro* inhibition of amylolytic enzymes. These commercial EOs and the citrus-derived EOs extracts were assessed for IC_{50} against α-amylase and α-glucosidase. Citrus EOs and their compounds did not exhibit strong α-amylase inhibitory activity (IC_{50} > 2 mg/mL), whereas Active Ingredient had an IC_{50} value of 0.008 ± 0.001 mg/mL. On the other hand, the EOs and some selected compounds exhibited potent α-glucosidase inhibitory activity with IC_{50} values within the concentration range (0.02 to 2 mg/mL). Active Ingredient had an IC_{50} of 0.11 mg/mL against α-glucosidase, whereas the IC_{50} values of the EOs extract were above 1 mg/mL. The IC_{50} values of the selected compounds are shown in Table 3.

The selected compounds have shown inhibition only for α-glucosidase within the concentration range used; therefore, they were analysed further for additional kinetic inhibition experiments against α-glucosidase. Table 3 shows the inhibitor constant (K_i) and the mode of inhibition of these compounds. These data suggested that the selected compounds exhibited competitive inhibition of α-glucosidase. For Active Ingredient, carveol, geraniol, and valencene, as presented in Table S2 (supplementary document), we observed an increase in the K_m value while the V_{max} remained unchanged, which indicates competitive inhibition [8]. The K_i is a better indication of how potent an inhibitor is; the lower the K_i value, the more powerful the inhibitor is [8, 58]. Therefore, the order of the potency of the inhibitory compounds is as follows: Active Ingredient > valencene > carveol > geraniol > limonene > linalool > nerol, with Active Ingredient being the most potent and nerol the least potent inhibitor. Valencene, carveol, and geraniol were selected as promising compounds for further studies. The kinetic parameters used to determine the mode of inhibition of Active Ingredient, carveol, geraniol, and valencene are shown in Table S2 in the supplementary data.

The compounds' *in vitro* inhibitory constants (K_i) correlated positively with their *in silico*-determined binding affinities; Pearson's correlation coefficient was 0.7708, indicating a highly positive correlation between the molecular docking and *in vitro* inhibition assay results, as shown in Figure 1.

A review by Kury *et al.* (2021) has elaborated on the antidiabetic effects of some essential oil compounds; fewer studies have investigated these compounds' inhibitory action against amylolytic enzymes [59]. The K_i values and the mode of inhibition of these compounds against α-glucosidase have not yet been explored in the literature. However, Active Ingredient has been investigated, and in correlation with the current study, it has been reported to be a competitive inhibitor of α-glucosidase [60, 61].

3.5. Molecular dynamic investigation of Active Ingredient and the selected compounds with α-glucosidase

Molecular dynamic simulations were investigated to further examine the binding interactions of the selected compounds and α-glucosidase throughout 100 ns. Among the selected essential oils, valencene, carveol, and geraniol exhibited more potent *in vitro* inhibitory activity against α-glucosidase, with K_i values of 0.33, 0.53 and 0.56 mg/mL, respectively. The abovementioned compounds were chosen for molecular dynamic investigation, while Active Ingredient (K_i of 0.10 mg/mL) was used for comparison as the standard inhibitor of α-glucosidase. MD was used to determine and generate the total binding energy ΔG_{bind}, the average of RMSD, RMSF, RoG, and SASA. MD parameters are shown in Table 4, and Figure 2 illustrates the changes over the simulation time.

The ΔG_{bind} was generated and presented in Table 4 for the interaction between α-glucosidase and the selected compounds. Active Ingredient had a more negative value, followed by geraniol, valencene and carveol. The order correlated with the docking scores in Table 3, where the more negative value indicates stronger binding affinity and stable complex between ligand and α-glucosidase [62]. In addition, the 2D Ligand-Protein interactions were plotted using LigPlot to determine the type of interactions formed after 100ns for each compound. As shown in Figure 3, hydrophobic interactions were predominantly observed in all compounds, with some shifts in the binding key residues for each compound. It was also observed that hydrogen bonds were formed between Active Ingredient with Asp408, carveol with Glu276, and geraniol with Arg356. Despite the lack of

hydrogen bond interactions in valencene, it presented stronger binding energy than carveol, which correlates with its smaller K_i value.

RMSD values were measured to analyse the conformational stability and rigidity of the ligandprotein complexes, and the values are presented in Table 4. The mean RMSD value of the apo α-glucosidase was higher than the complexes with Active Ingredient, valencene and carveol. Figure 2A illustrates the RMSD changes over time throughout the 100 ns. The RMSD initially increased dramatically before maintaining a stable state with slight deviations at different RMSD values and time. The RMSD profile in Figure 2A shows that the complexes reached equilibrium at values below 2.5 Å, which indicates the stable state of the complexes; the lower the RMSD, the greater the stability and rigidity [63-65]. Therefore, the order of complex stability and rigidity in this study is as follows: valencene > Active Ingredient > carveol > geraniol.

RMSF values were measured to analyse the flexibility of the protein backbone throughout 100 ns. A high RMSF value indicates more flexibility and mobility and less stability between the ligand and protein, while a low RMSF value is associated with the residue maintaining a stable position, being more rigid and having less fluctuation [66, 67]. Figure 2B illustrates the RMSF values to indicate the flexibility of individual residues of α-glucosidase over time. The active site of α-glucosidase is found around residues shown in Figures 2 and 3 [67]. Complex with Active Ingredient illustrated the lowest RMSF in the active site region (Figure 2B), which indicates more stability/rigidity and less fluctuation and correlates with Active Ingredient as a potent competitive inhibitor of α-glucosidase (Table 3).

RoG was measured to analyse the structural compactness of α-glucosidase and the liability of the complexes. A low RoG value indicates tight packing associated with a more stable and compact structure, while a high RoG value indicates less tight packing, greater flexibility and less stable configuration [68]. Figure 2C illustrates that the RoG of the complexes initially increased rapidly before reaching a stable state. The mean RoG values of the complexes (Table 4) show that apo α-glucosidase has the lowest value than ligand-protein complexes, showing conformational changes upon ligand binding to α-glucosidase. The order of complex stability and compactness in this study is as follows: Active Ingredient > valencene > carveol > geraniol.

SASA is measured to quantify the surface area of α-glucosidase accessible to solvent molecules [69]. SASA helps to understand the stability, molecular interactions and function of proteins relevant to protein folding, ligand binding, and conformational changes [70]. The apo α-glucosidase has a higher mean SASA value than the complex with Active Ingredient, valencene and carveol, indicating that α-glucosidase has a rigid binding affinity with these ligands, corresponding to folded and stable structure compared to apo α-glucosidase. In contrast, the complex with geraniol has a higher SASA value than the apo α-glucosidase, which indicates less stable/rigid binding affinity, and unfolded structure compared to the apo α-glucosidase.

The MD parameters in Table 4 correlated positively throughout the simulation study. Complex with geraniol has the highest mean values for the measured parameters compared to the apo α-glucosidase and other complexes. Complexes with Active Ingredient, valencene, and carveol exhibited a more stable structure than geraniol in terms of rigidity, compactness, and fluctuation.

3.6. Inhibition of the amylolytic enzyme cocktail by Active Ingredient or potent EOs

The inhibition of an amylolytic enzyme cocktail by Active Ingredient, carveol, geraniol, and valencene was assessed by determining the IC_{50} value that inhibited the production of the reducing sugar through the DNS method and the IC_{50} that inhibited the amount of glucose released through the GOPOD method, shown in Figure 4. Active Ingredient inhibited the activity of the enzyme cocktail at lower concentrations with IC_{50} values of 2.50 and 2.10 µg/mL for the inhibition of α-amylase and α-glucosidase activities, respectively. The result shows that Active Ingredient strongly inhibits the activities of both enzymes, and its action may lead to the accumulation of undigested starch in the colon associated with abdominal discomfort [71]. Therefore, a slight inhibition of α-amylase and potent inhibition of α-glucosidase is preferable because it leads to high production of total reducing sugars and a low amount of glucose released; furthermore, it reduces the accumulation of undigested starch and its associated side effects [15, 72].

Carveol, geraniol, and valencene did not inhibit α-amylase activity at the highest inhibitor concentration, with some EOs showing slight activation of the enzyme instead of inhibition. On the other hand, the promising compounds show a dose-dependent inhibition of α-glucosidase activity, with IC_{50} values of 1.32, 1.63, and 1.70 mg/mL for carveol, geraniol, and valencene, respectively. The above result is ideal because it minimises adverse effects associated with

undigested starch and reduces the amount of glucose released. Therefore, these compounds could be potential antidiabetic agents for managing type 2 diabetes.

3.7. Combined effects of Active Ingrediet and potent EOs against the amylolytic enzyme cocktail

The combination effects of the selected compounds against the amylolytic enzyme cocktail were assessed by mixing Active Ingredient with each promising EOs at different inhibitory potency ratios. An approximation of IC_{30} (0.625 µg/mL), IC_{50} (3.125 µg/mL), and IC_{75} (12.5 µg/mL) of Active Ingredient were each mixed with IC_{30} (0.5 mg/mL), IC_{50} (1 mg/mL) and IC_{75} (2 mg/mL) of carveol, geraniol or valencene, yielding nine combinations. A combination index (CI) and a CI-isobologram were then generated from the results (Figure S5 and Tables 5 & 6). According to drug synergism studies, CI<1, CI=1, and CI>1 indicate synergism, additive, and antagonism effects, respectively [41].

Combining Active Ingredient with carveol, geraniol, or valencene exhibited an antagonistic effect on α-amylase inhibition, with the combination index (CI) being higher than 1.45. No CI-isobologram was generated due to all the points being outside the graph. Active Ingredient combined with carveol had a powerful antagonistic effect with CI higher than 10. The observed result is ideal as these drug combinations lead to the reduction of the amount of undigested starch by reducing the strong α-amylase inhibitory activity of Active Ingredient and producing more reducing sugars.

On the other hand, combining Active Ingredient with carveol or geraniol exhibited a synergistic effect for α-glucosidase inhibition, and some were nearly additive with CI values lower than 1 (Table 5). Figures S5A and B clearly show the presence of all nine points inside the graph to promote synergistic or nearly additive effects on α-glucosidase inhibition. The outcome correlates with the ideal results expected because it reduces glucose released to the bloodstream, thus possibly minimising postprandial hyperglycemia. However, the combination of Active Ingredient with valencene exhibited antagonistic and additive effects on α-glucosidase inhibition, with most CI values higher than 1.20.

Combining Act.Ing. with carveol and geraniol (12.5 µg/mL: 2 mg/mL) showed the ideal results because of the desired antagonistic effect on α-amylase inhibition, promoting the production of reducing sugars, and a more substantial synergistic effect on α-glucosidase inhibition, reducing the

3.8. Quantification of undigested starch

The starch-iodine method was used to further quantify the amount of starch residues after the enzymatic reactions. This method was used to identify further which of the two ideal combinations is associated with minimal starch residues. The percentage of undigested starch was calculated using the formula in Equation 3 (see 2.12). Figure 4 illustrates the % undigested starch along with % inhibition of reducing sugar released (RSR) and glucose released (GR) for the combination of Act.Ing. with carveol and geraniol at the ratio (12.5 µg/mL 2 mg/mL), which showed stronger antagonistic and synergistic effect for RS and glucose production, respectively. The combinations were compared to the impact of the single compounds (Figure 5).

Act.Ing. had the highest amount of undigested starch (92%), possibly associated with its strong inhibition of RSR, leading to less starch digestion. Carveol and geraniol exhibited no inhibition of RSR, with increased α-amylase activity, leading to less undigested starch (3 and 17%, respectively). Both combinations of Act.Ing. with carveol or geraniol led to a slight increase in the inhibition of GR from 65% to 67% and 69% for the combination with carveol or geraniol, respectively. Combining Act.Ing. with carveol significantly decreased undigested starch from 92% to 33%, whereas combining Act.Ing. with geraniol decreased undigested starch to 79%. A similar study investigated the effect of flavonoids and Act.Ing. on the digestibility of starch; the authors reported a decrease in starch due to the presence of Act.Ing. because of its strong inhibitory activity on α-amylase [73].

Other studies have speculated that in addition to the inhibition of α-amylase, the hydrophobic interactions between the inhibitor and the helical structure of starch may also affect the digestibility of starch [73-75]. However, the authors reported no binding interaction between Act.Ing. and starch, thus concluding that the effect was solely due to the strong inhibitory activity of Act.Ing. on α-amylase.

3.9. Particle size determination of the starch hydrolysate

The average particle size of hydrolysate from the inhibition reaction with Act.Ing., carveol and a combination of Act.Ing. and carveol was used to validate the amount of undigested starch. As indicated in Table 4, the average particle sizes were 129 and 36 nm for the reaction with Act.Ing. alone and in combination with carveol, respectively. The average particle sizes were compared to

the starch solution alone, which had an average size of 164 nm. The average size of a starch solution is reported to range between 40 and 300 nm depending on conditions and aggregations [76].

The data in Table 7 correlated with the % undigested starch in Figure 5, where Active Ingredient had a high undigested starch compared to the combination with carveol. The large particle size in Active Ingredient is due to the undigested starch associated with strong inhibition of α-amylase. In contrast, a significant decrease in average particle size was observed in the combination of Active Ingredient with carveol, associated with decreased inhibition of α-amylase and hydrolysis of starch into smaller molecules.

4. CONCLUSION

The current study highlights the AGI activity of EOs derived from citrus peels using in silico and in vitro approaches. The EOs demonstrated a more potent inhibitory effect on α-glucosidase compared to α-amylase, which could help reduce side effects linked to undigested starch while lowering glucose release. MD simulations revealed that carveol, geraniol, and valencene had stable and flexible interactions with α-glucosidase, leading to compact complex formation. The combination of Active Ingredient with either carveol or geraniol produced antagonistic and synergistic effects on α-amylase and α-glucosidase, respectively, potentially alleviating side effects associated with undigested starch and enhancing therapeutic outcomes. Overall, the findings suggest that citrus peel-derived EOs could be promising antidiabetic agents. Furthermore, these compounds can be sourced from citrus peel waste, aligning with circular economy principles and offering a cost-effective solution for increased accessibility. However, additional in vitro and in vivo studies are needed to validate these results.

Author contributions

Kadima Samuel Tshiyoyo: *In silico* and *In vitro* investigation, Visualisation, Formal analysis, Data curation, Writing – Original Draft, Writing – Review & Editing. **Abdullahi Ahmed Yusuf:** GC-MS methodology and materials. **Ali Rabbad:** Molecular dynamic simulations methodology and materials. **Samkelo Malgas:** Supervision, Conceptualisation, Formal analysis, Methodology, Funding acquisition, Project administration, Review & Editing.

Acknowledgments

The authors acknowledge the Center of High-Perfomance Computing (CHPC), Cape Town, South Africa, for the platform to conduct the computational part of the study.

Declaration of interests

The authors declare that they have no known competing financial interests or personal relationships that could have appeared to influence the work.

Funding

This study was supported by the competitive support for unrated Researchers grant No 138084 awarded by the National Research Foundation (NRF), South Africa.

Supplementary material

The supplementary document associated with this article is attached.

Data availability

Data sets generated from this work are available upon request.

Declaration of generative AI and AI-assisted technologies in the writing process

During the preparation of this work, the authors used Grammarly: Free AI Writing Assistance to improve grammar and the tone of the language in the manuscript. After using this tool/service, the authors reviewed and edited the content as needed and take full responsibility for the content of the publication.

5. References

1. Egan, A.M. and S.F. Dinneen, *What is diabetes?* Medicine, 2019. **47**(1): p. 1-4.
2. Quondamatteo, F., *Skin and diabetes mellitus: what do we know?* Cell and tissue research, 2014. **355**: p. 1-21.
3. Mohan, V., et al., *Epidemiology of type 2 diabetes: Indian scenario.* Indian J Med Res, 2007. **125**(3): p. 217-30.
4. IDF, *International Diabetes Federation Diabetes Atlas 2021*. 2021.
5. Forouhi, N.G. and N.J. Wareham, *Epidemiology of diabetes.* Medicine, 2022.
6. Kokil, G.R., et al., *Type 2 diabetes mellitus: limitations of conventional therapies and intervention with nucleic acid-based therapeutics.* Chemical Reviews, 2015. **115**(11): p. 4719-4743.
7. Deng, X.-Y., et al., *Synthesis and bioactivities evaluation of oleanolic acid oxime ester derivatives as α-glucosidase and α-amylase inhibitors.* Journal of Enzyme Inhibition and Medicinal Chemistry, 2022. **37**(1): p. 451-461.
8. Voet, D. and J.G. Voet, *Biochemistry*. 2021: John Wiley & Sons.
9. Vihinen, M. and P. Mantsiila, *Microbial amylolytic enzyme.* Critical reviews in biochemistry and molecular biology, 1989. **24**(4): p. 329-418.
10. Tiwari, S., et al., *Amylases: an overview with special reference to alpha amylase.* J Global Biosci, 2015. **4**(1): p. 1886-1901.
11. Jones, M., et al., *Cambridge International AS and A Level Biology Coursebook with CD-ROM*. 2014: Cambridge University Press.
12. Martin, A.E. and P.A. Montgomery, *Active Ingredient: An α-glucosidase inhibitor.* American journal of health-system pharmacy, 1996. **53**(19): p. 2277-2290.
13. Sensoy, I., *A review on the food digestion in the digestive tract and the used in vitro models.* Current research in food science, 2021. **4**: p. 308-319.
14. Turner, N., et al., *Repurposing drugs to target the diabetes epidemic.* Trends in pharmacological sciences, 2016. **37**(5): p. 379-389.
15. Tolmie, M., M.J. Bester, and Z. Apostolides, *Inhibition of α-glucosidase and α-amylase by herbal compounds for the treatment of type 2 diabetes: a validation of in silico reverse docking with in vitro enzyme assays.* Journal of Diabetes, 2021. **13**(10): p. 779-791.
16. Petrovska, B.B., *Historical review of medicinal plants' usage.* Pharmacognosy reviews, 2012. **6**(11): p. 1.
17. Zou, Z., et al., *Antioxidant activity of Citrus fruits.* Food chemistry, 2016. **196**: p. 885-896.
18. Cui, J., et al., *The structure–property relationships of acid-and alkali-extracted grapefruit peel pectins.* Carbohydrate polymers, 2020. **229**: p. 115524.
19. Liu, N., et al., *A review of chemical constituents and health-promoting effects of citrus peels.* Food Chemistry, 2021. **365**: p. 130585.
20. Chavan, P., A.K. Singh, and G. Kaur, *Recent progress in the utilization of industrial waste and by-products of citrus fruits: A review.* Journal of Food Process Engineering, 2018. **41**(8): p. e12895.
21. Mahato, N., et al., *Biotransformation of citrus waste-I: Production of biofuel and valuable compounds by fermentation.* Processes, 2021. **9**(2): p. 220.
22. Bora, H., et al., *Citrus essential oils (CEOs) and their applications in food: An overview.* Plants, 2020. **9**(3): p. 357.
23. Nakatsu, T., et al., *Biological activity of essential oils and their constituents.* Studies in natural products chemistry, 2000. **21**: p. 571-631.
24. Ambrosio, C., et al., *Unraveling the selective antibacterial activity and chemical composition of citrus essential oils.* Scientific reports, 2019. **9**(1): p. 1-13.

25. Mahato, N., et al., *Citrus essential oils: Extraction, authentication and application in food preservation.* Critical reviews in food science and nutrition, 2019. **59**(4): p. 611-625.
26. Majouli, K., et al., *Antioxidant activity and α-glucosidase inhibition by essential oils from Hertia cheirifolia (L.).* Industrial Crops and Products, 2016. **82**: p. 23-28.
27. Salazar, M.O., et al., *New α-glucosidase inhibitors from a chemically engineered essential oil of Origanum vulgare L.* Industrial Crops and Products, 2020. **156**: p. 112855.
28. Sadka, A., et al., *Primary metabolism in citrus fruit as affected by its unique structure.* Frontiers in plant science, 2019. **10**: p. 1167.
29. Lu, Q., et al., *Peel oils from three Citrus species: volatile constituents, antioxidant activities and related contributions of individual components.* J Food Sci Technol, 2019. **56**(10): p. 4492-4502.
30. Stein, S., et al., *The NIST mass spectral search program for the nist/epa/nih mass spectra library. Standard Reference Data Program of the National Institute of Standards and Technology, Gaithersburg, MD, US, 2011*. 2021.
31. Daina, A., O. Michielin, and V. Zoete, *SwissADME: a free web tool to evaluate pharmacokinetics, drug-likeness and medicinal chemistry friendliness of small molecules.* Scientific reports, 2017. **7**(1): p. 42717.
32. Morris, G.M., et al., *AutoDock4 and AutoDockTools4: Automated docking with selective receptor flexibility.* Journal of computational chemistry, 2009. **30**(16): p. 2785-2791.
33. Dallakyan, S. and A.J. Olson, *Small-molecule library screening by docking with PyRx.* Chemical biology: methods and protocols, 2015: p. 243-250.
34. Yousuf, M., K. Mammadova, and L. Khan, *Homology Modeling of α-Glucosidase Enzyme: 3D Structure Prediction.* Bioinformatics Review, 2018. **4**(11): p. 09-14.
35. Megazyme, *GOPOD REAGENT ENZYMES (For the preparation of GOPOD determination reagents)* 2019.
36. Pettersen, E.F., et al., *UCSF Chimera—a visualization system for exploratory research and analysis.* Journal of computational chemistry, 2004. **25**(13): p. 1605-1612.
37. Case, D.A., et al., *The Amber biomolecular simulation programs.* Journal of computational chemistry, 2005. **26**(16): p. 1668-1688.
38. Rabbad, A.H., et al., *Microbes, not humans: exploring the molecular basis of Pseudouridimycin selectivity towards bacterial and not human RNA polymerase.* Biotechnology letters, 2019. **41**: p. 115-128.
39. Oduro-Kwateng, E., A.H. Rabbad, and M.E. Soliman, *The Juxtaposition of Allosteric and Catalytic Inhibition in PLK1: Tradeoff for Chemotherapy and Thermodynamic Profiles of KBJK557 and BI 6727.* Journal of Computational Biophysics and Chemistry, 2024. **23**(3): p. 379-401.
40. H. Rabbad, A., C. Agoni, and M. E. Soliman, *Structural Insights into the role of pseudouridimycin binding in disruption of bacterial RNA polymerase bridge helix conformational arrangement.* Current Pharmaceutical Biotechnology, 2023. **24**(4): p. 562-569.
41. Chou, T.-C., *Theoretical basis, experimental design, and computerized simulation of synergism and antagonism in drug combination studies.* Pharmacological reviews, 2006. **58**(3): p. 621-681.
42. Xiao, Z., R. Storms, and A. Tsang, *A quantitative starch? Iodine method for measuring alpha-amylase and glucoamylase activities.* Analytical biochemistry, 2006. **351**(1): p. 146-148.
43. Singh, B., et al., *Insights into the chemical composition and bioactivities of citrus peel essential oils.* Food Research International, 2021. **143**: p. 110231.
44. Brahmi, F., et al., *Chemical and biological characterization of essential oils extracted from citrus fruits peels.* Materials Today: Proceedings, 2021. **45**: p. 7794-7799.
45. Satari, B., et al., *Process optimization for citrus waste biorefinery via simultaneous pectin extraction and pretreatment.* BioResources, 2017. **12**(1): p. 1706-1722.

46. Bhandari, D.P., et al., *Volatile compounds and antioxidant and antimicrobial activities of selected citrus essential oils originated from Nepal.* Molecules, 2021. **26**(21): p. 6683.
47. Vasquez-Gomez, K.L., et al., *Characterization of Essential Oils from the Skin of Citrus limetta Risso, Citrus limetta Sp., Citrus reticulata and Citrus sinensis Grown in Northeastern Peru.* 2023.
48. Hérent, M.-F., V. De Bie, and B. Tilquin, *Determination of new retention indices for quick identification of essential oils compounds.* Journal of Pharmaceutical and biomedical Analysis, 2007. **43**(3): p. 886-892.
49. Saeidi, M., et al., *Comparative volatile composition, antioxidant and cytotoxic evaluation of the essential oil of Zhumeria majdae from south of Iran.* Iranian Journal of Basic Medical Sciences, 2019. **22**(1): p. 80.
50. Benchama, Z., et al., *Chemical composition and antibacterial activity of the essential oils of Asphodelus microcarpus Salzm. & Viv. growing wild at different sites in Morocco: ADME-Tox, molecular docking and molecular dynamics simulations.* Journal of Essential Oil Research, 2024: p. 1-17.
51. Zhang, W., et al., *Peel Essential Oil Composition and Antibacterial Activities of Citrus x sinensis L. Osbeck 'Tarocco'and Citrus reticulata Blanco.* Horticulturae, 2022. **8**(9): p. 793.
52. Ghadiri, K., et al., *Response surface methodology for optimization of supercritical fluid extraction of orange peel essential oil.* Pharmaceutical and Biomedical Research, 2020. **6**(4): p. 303-312.
53. Li, C., et al., *Variation in compositions and biological activities of essential oils from four citrus species: Citrus limon, Citrus sinensis, Citrus paradisi, and Citrus reticulata.* Chemistry & Biodiversity, 2022. **19**(4): p. e202100910.
54. Javed, S., et al., *Phytochemistry, GC-MS analysis, antioxidant and antimicrobial potential of essential oil from five citrus species.* Journal of Agricultural Science, 2014. **6**(3): p. 201.
55. Sympli, H.D., *Estimation of drug-likeness properties of GC–MS separated bioactive compounds in rare medicinal Pleione maculata using molecular docking technique and SwissADME in silico tools.* Network Modeling Analysis in Health Informatics and Bioinformatics, 2021. **10**(1): p. 14.
56. Liu, W., H. Wang, and F. Meng, *In silico modeling of aspalathin and nothofagin against SGLT2.* Journal of Theoretical and Computational Chemistry, 2015. **14**(08): p. 1550056.
57. García-Ortegón, M., et al., *DOCKSTRING: easy molecular docking yields better benchmarks for ligand design.* Journal of chemical information and modeling, 2022. **62**(15): p. 3486-3502.
58. Kim, H.-Y., et al., *Anti-diabetic effect of the lupinalbin A compound isolated from Apios americana: In vitro analysis and molecular docking study.* Biomedical Reports, 2021. **14**(4): p. 1-5.
59. Al Kury, L.T., et al., *In vitro and in vivo antidiabetic potential of monoterpenoids: An update.* Molecules, 2021. **27**(1): p. 182.
60. Ni, M., et al., *Inhibitory mechanism of vitexin on α-glucosidase and its synergy with Active Ingredient.* Food Hydrocolloids, 2020. **105**: p. 105824.
61. Tshiyoyo, K.S., *In silico docking and ADMET studies on clinical targets for type 2 diabetes correlated to in vitro inhibition of α glucosidase and pancreatic α-amylase by curcumin, 18α glycyrrhetinic acid, rosmarinic acid, and quercetin*, in *Biochemistry, Genetics and Microbiology*. 2022, University of Pretoria: Pretoria, South Africa.
62. Uzzaman, M., et al., *Medicinal and toxicological investigation of some common NSAIDs; A computer-aided drug design approach.* Journal of Molecular Structure, 2023. **1292**: p. 136124.
63. Ahmed, S., et al., *Molecular docking and dynamics simulation of natural compounds from betel leaves (Piper betle L.) for investigating the potential inhibition of alpha-amylase and alpha-glucosidase of type 2 diabetes.* Molecules, 2022. **27**(14): p. 4526.
64. Wu, N., et al., *Elucidation of protein–ligand interactions by multiple trajectory analysis methods.* Physical Chemistry Chemical Physics, 2024. **26**(8): p. 6903-6915.

65. Rampogu, S., et al., *Molecular docking and molecular dynamics simulations discover curcumin analogue as a plausible dual inhibitor for SARS-CoV-2.* International Journal of Molecular Sciences, 2022. **23**(3): p. 1771.
66. Ghahremanian, S., et al., *Molecular dynamics simulation approach for discovering potential inhibitors against SARS-CoV-2: A structural review.* Journal of molecular liquids, 2022. **354**: p. 118901.
67. Asadi, M., et al., *Synthesis, α-glucosidase inhibitory activity, and molecular dynamic simulation of 6-chloro-2-methoxyacridine linked to triazole derivatives.* Scientific Reports, 2024. **14**(1): p. 17338.
68. Lobanov, M.Y., N. Bogatyreva, and O. Galzitskaya, *Radius of gyration as an indicator of protein structure compactness.* Molecular Biology, 2008. **42**: p. 623-628.
69. Anuar, N.F.S.K., et al., *Molecular docking and molecular dynamics simulations of a mutant Acinetobacter haemolyticus alkaline-stable lipase against tributyrin.* Journal of Biomolecular Structure and Dynamics, 2021. **39**(6): p. 2079-2091.
70. Durham, E., et al., *Solvent accessible surface area approximations for rapid and accurate protein structure prediction.* Journal of molecular modeling, 2009. **15**: p. 1093-1108.
71. Dong, Y., et al., *Reducing the intestinal side effects of Active Ingredient by baicalein through the regulation of gut microbiota: An in vitro study.* Food Chemistry, 2022. **394**: p. 133561.
72. Mabate, B., et al., *A Combination Approach in Inhibiting Type 2 Diabetes-Related Enzymes Using Ecklonia radiata Fucoidan and Active Ingredient.* Pharmaceutics, 2021. **13**(11): p. 1979.
73. Yang, J.-P., H. He, and Y.-H. Lu, *Four flavonoid compounds from Phyllostachys edulis leaf extract retard the digestion of starch and its working mechanisms.* Journal of Agricultural and Food Chemistry, 2014. **62**(31): p. 7760-7770.
74. Shen, W., Y. Xu, and Y.-H. Lu, *Inhibitory effects of Citrus flavonoids on starch digestion and antihyperglycemic effects in HepG2 cells.* Journal of agricultural and food chemistry, 2012. **60**(38): p. 9609-9619.
75. Takahama, U. and S. Hirota, *Fatty acids, epicatechin-dimethylgallate, and rutin interact with buckwheat starch inhibiting its digestion by amylase: Implications for the decrease in glycemic index by buckwheat flour.* Journal of Agricultural and Food Chemistry, 2010. **58**(23): p. 12431-12439.
76. Chakraborty, S., et al., *Solution properties of starch nanoparticles in water and DMSO as studied by dynamic light scattering.* Carbohydrate polymers, 2005. **60**(4): p. 475-481.

List of tables

Table 1. Chemicals identified from essential oils of two citrus peels.

	Retention time (min)	Compound	Retention index	Extracts			
				C. reticulata		*C. sinensis*	
				Hexane	EA	Hexane	EA
1	7.696	α-Pinene	1003	+	--	+	--
2	8.586	β-Pinene	1039	+	--	+	--
3	8.875	β-myrcene	1050	+	--	+	--
4	9.412	α-Terpinene	1072	+	--	+	--
5	9.773	Limonene	1087	+	--	+	--
6	10.209	γ-Terpinene	1105	+	--	--	--
7	10.714	α-Terpinolene	1126	+	+	--	--
8	10.889	Linalool	1133	+	+	+	+
9	11.261	Trans-p-Mentha-2,8-dienol	1148	+	+	--	+
10	11.501	Cis-p-Mentha-2,8-dienol	1158	+	+	--	+
11	11.554	Limonene oxide	1161	+	--	--	--
12	12.218	Terpin-4-ol	1188	--	---	+	+
13	12.425	α-Terpineol	1197	+	+	+	+
14	12.844	Trans-carveol	1223	+	+	--	+
15	12.946	Nerol	1229	+	+	--	+
16	13.020	Cis-carveol	1234	+	+	--	+
17	13.147	Z-Citral	1243	+	--	+	+
18	13.236	Carvone	1249	+	--	--	+
19	13.317	Geraniol	1254	+	+	--	+
20	13.564	E-Citral	1270	+	---	+	+
21	13.572	Linalool oxide	1271	--	+	--	--
22	13.653	Isopiperitenone	1276	--	+	--	+

23	13.698	Perillaldehyde	1279	+	--	--	+
24	13.906	p-Mentha-1(7),8(10)-dien-9-ol	1293	+	+	--	+
25	14.649	Limonene-1,2-diol	1339	--	+	--	+
26	14.941	Neryl acetate	1357	+	--	--	--
27	15.349	α-Copaene	1382	+	--	--	--
28	15.589	Germacrene B or β-copaene	1397	+	+	--	--
29	15.855	Limonen-10-yl acetate	1412	+	+	--	+
30	16.223	Trans-caryophellene	1434	+	--	--	--
31	16.372	Germacrene D	1442	+	--	--	--
32	17.437	Valencene	1506	--	--	+	+
33	17.48	Farnesene	1509	+	--	--	--
34	17.824	Δ-Cadinene	1534	+	+	--	+
35	18.171	Elemol	1559	+	+	--	---
36	18.268	Nerolidol	1566	+	+	--	--
37	19.151	γ-Gurjunene	1640	--	--	--	+
38	19.831	β-Sinensal	1705	+	+	--	+
39	20.041	Farnesol	1728	+	--	--	--
40	20.115	Dihydrocarvyl acetate	1736	+	+	--	--
41	20.257	Trans-farnesal	1751	--	--	--	+
42	20.365	α-Sinensal	1763	+	+	--	+
43	21.561	D-nerolidol	1902	--	--	--	+

Ethyl acetate (EA) ; Present (+); Absent (--)

Table 2. Pharmacokinetic properties of Active Ingredient and essential oils identified in the citrus peels.

Compound	**GI Absorption**	**Bioavailability**	**CYP inhibitor**	**Pgp substrate**	**BBB permeant**
Active Ing	Low	0.17	No (0/5)	Yes	No
Carveol	High	0.55	No (0/5)	No	Yes
Carvone	High	0.55	No (0/5)	No	Yes
Germacrene D	Low	0.55	No (0/5)	No	No
Geraniol	High	0.55	No (0/5)	No	Yes
Limonene	Low	0.55	Yes (1/5)	No	Yes
Linalool	High	0.55	No (0/5)	No	Yes
Nerol	High	0.55	No (0/5)	No	Yes
Terpineol	High	0.55	No (0/5)	No	Yes
Sinensal	High	0.55	Yes (1/5)	No	Yes
Valencene	Low	0.55	Yes (2/5)	No	No

Table 3. Binding affinity, IC_{50} values, K_i, and mode of inhibition (MOI) of Active Ingredient and commercially available citrus essential oils against α-glucosidase.

Compound	**Binding affinity (kcal/mol)**	IC_{50} **(mg/mL)**	K_i **(mg/mL)**	**Mode of Inhibition**
Active Ing.	-7.5	0.11 ± 0.01	0.10 ± 0.01	Competitive
Valencene	-7.4	0.65 ± 0.01	0.33 ± 0.04	Competitive
Carveol	-7.2	0.54 ± 0.02	0.53 ± 0.02	Competitive
Limonene	-6.5	1.51 ± 0.02	1.10 ± 0.07	Competitive
Geraniol	-5.9	0.71 ± 0.05	0.56 ± 0.02	Competitive
Linalool	-5.8	1.88 ± 0.18	0.90 ± 0.03	Competitive
Nerol	-5.5	1.08 ± 0.04	1.06 ± 0.08	Competitive

Table 4. Total binding energy and conformational dynamics results between selected compounds and α-glucosidase throughout 100 ns.

Compound	**ΔGbind (kcal/mol)**	**Mean of RMSD (Å)**	**Mean of RMSF (Å)**	**Mean of RoG (Å)**	**Mean of SASA (Å^2)**
Apo	---	2.24661	1.15194	24.39143	21691.71852
Active Ing.	-32.8157	2.01614	1.19694	24.46236	21140.78108
Valencene	-18.4480	1.82515	1.09036	24.54001	21180.15473
Carveol	-17.6714	2.19487	1.09283	24.5626	21678.30757
Geraniol	-20.7200	2.27427	1.29004	24.6047	21708.57684

Table 5. Combination study of Active Ingredient and essential oils on amylolytic enzymes cocktail to inhibit total reducing sugars and glucose released.

Combination points	Acarbose (µg/mL) : EOs (mg/mL)	Active Ing.: Carveol				Active Ing.: Geraniol				Active Ing.: Valencene			
		Reducing sugars released		Glucose released		Reducing sugars released		Glucose released		Reducing sugars released		Glucose released	
		% Inhibition	CI	% Inhibition	CI	% Inhibition	CI	% Inhibition	CI	% Inhibition	CI	% Inhibition	CI
1	12.5: 2	67.51	> 10	78.21	0.62	64.98	> 10	81.25	0.38	26.67	> 10	57.98	3.65
2	12.5: 1	63.82	> 10	76.17	0.66	69.70	> 10	77.64	0.52	49.68	5.09	66.83	1.55
3	12.5: 0.5	69.82	> 10	74.34	0.72	72.45	> 10	77.35	0.50	63.93	2.56	67.66	1.35
4	3.125: 2	41.16	> 10	68.60	0.77	36.35	> 10	66.70	0.79	0.90	> 10	56.32	1.67
5	3.125: 1	39.54	> 10	59.96	1.09	42.55	> 10	62.83	0.80	20.01	6.31	49.72	2.08
6	3.125: 0.5	37.14	> 10	58.87	0.93	44.06	> 10	57.98	0.97	36.04	2.48	50.54	1.64
7	0.625: 2	14.51	> 10	65.17	0.72	11.90	3.03	62.89	0.73	0.26	> 10	53.53	1.22
8	0.625: 1	16.71	> 10	53.50	0.96	15.32	2.32	52.02	1.03	2.52	> 10	44.14	1.41
9	0.625: 0.5	19.81	> 10	46.88	0.96	20.49	1.81	47.26	0.94	10.36	3.16	33.34	2.17

CI: combination index

Table 6. Synergistic effects of combined Active Ingredient and essential oils on the amylolytic enzymes cocktail for the inhibition of reducing sugars and glucose released.

Combination points	Active Ing. (µg/mL): EOs (mg/ mL)	Active Ing.: Carveol		Active Ing.: Geraniol		Active Ing.: Valencene	
		Effect		Effect		Effect	
		Reducing sugars released	Glucose released	Reducing sugars released	Glucose released	Reducing sugars released	Glucose released
1	12.5: 2	Very strong antagonism	Synergism	Very strong antagonism	Synergism	Very strong antagonism	Strong Antagonism
2	12.5: 1		Synergism			Strong Antagonism	Antagonism
3	12.5: 0.5		Moderate Synergism			Antagonism	Moderate Antagonism
4	3.125: 2		Moderate Synergism		Moderate Synergism	Very strong antagonism	Antagonism
5	3.125: 1		Nearly Additive			Strong Antagonism	Antagonism
6	3.125: 0.5		Nearly Additive		Nearly Additive	Antagonism	Antagonism
7	0.625: 2		Moderate Antagonism	Antagonism	Moderate Synergism	Very strong antagonism	Moderate Antagonism
8	0.625: 1		Moderate Antagonism		Nearly Additive	Very strong antagonism	Moderate Antagonism
9	0.625: 0.5		Antagonism			Antagonism	Antagonism

Table 7. Average particle size and polydispersity index of starch hydrolysate.

Sample (hydrolysate)	**Average particle size Xave (nm)**	**Polydispersity (PDI)**
Starch only	163.62 ± 15.38	0.47 ± 0.01
No inhibitor	5.16 ± 0.34	0.29 ± 0.03
Act. Ing. as inhibitor	128.59 ± 18.16	0.44 ± 0.02
Carveol as inhibitor	7.30 ± 1.15	0.21 ± 0.01
Act. Ing. + carveol	36.17 ± 3.88	0.59 ± 0.01

Figure captions:

Figure 1. Graph of Autodock generated binding affinities vs the inhibitor constant (K_i) to show the relationship between molecular docking and in vitro results.

Figure 2. Molecular dynamic simulation for α-glucosidase and complexes with selected compounds throughout the 100 ns of the simulation time. Analysis of (A) root mean square deviation (RMSD); (B) root mean square fluctuations (RMSF); (C) radius of gyration (RoG) and (D) solvent accessible surface area (SASA).

Figure 3. Ligand-protein (α-glucosidase) interactions after 100 ns derived from MD simulations. The figure illustrates the spatial arrangement and interaction types between the surrounding protein residues and ligands; (A) Active Ingredient, (B) valencene, (C) carveol, and (D) geraniol.

Figure 4. Inhibition of amylolytic enzyme cocktail (α-amylase and α-glucosidase) by Active Ingredient (top left), carveol (top right), geraniol (bottom left), and valencene (bottom right). Two curves are shown in each plot, representing the inhibition of total reducing sugars (TRS) and glucose released (GR).

Figure 5. % Inhibition of reducing sugar released (RSR), % inhibition of glucose released (GR), and % undigested starch by Active Ingredient (12.5 µg/mL), carveol (2 mg/mL), geraniol (2 mg/mL), a combination of Active Ingredient: carveol, and a combination of Active Ingredient: geraniol. Values are represented as mean and SEM.

Figures

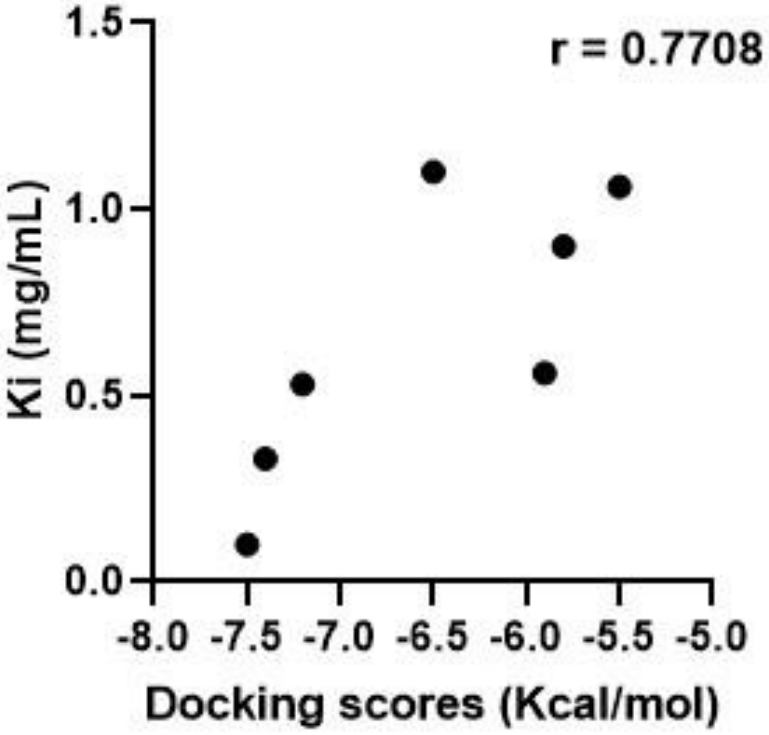

Figure 1.

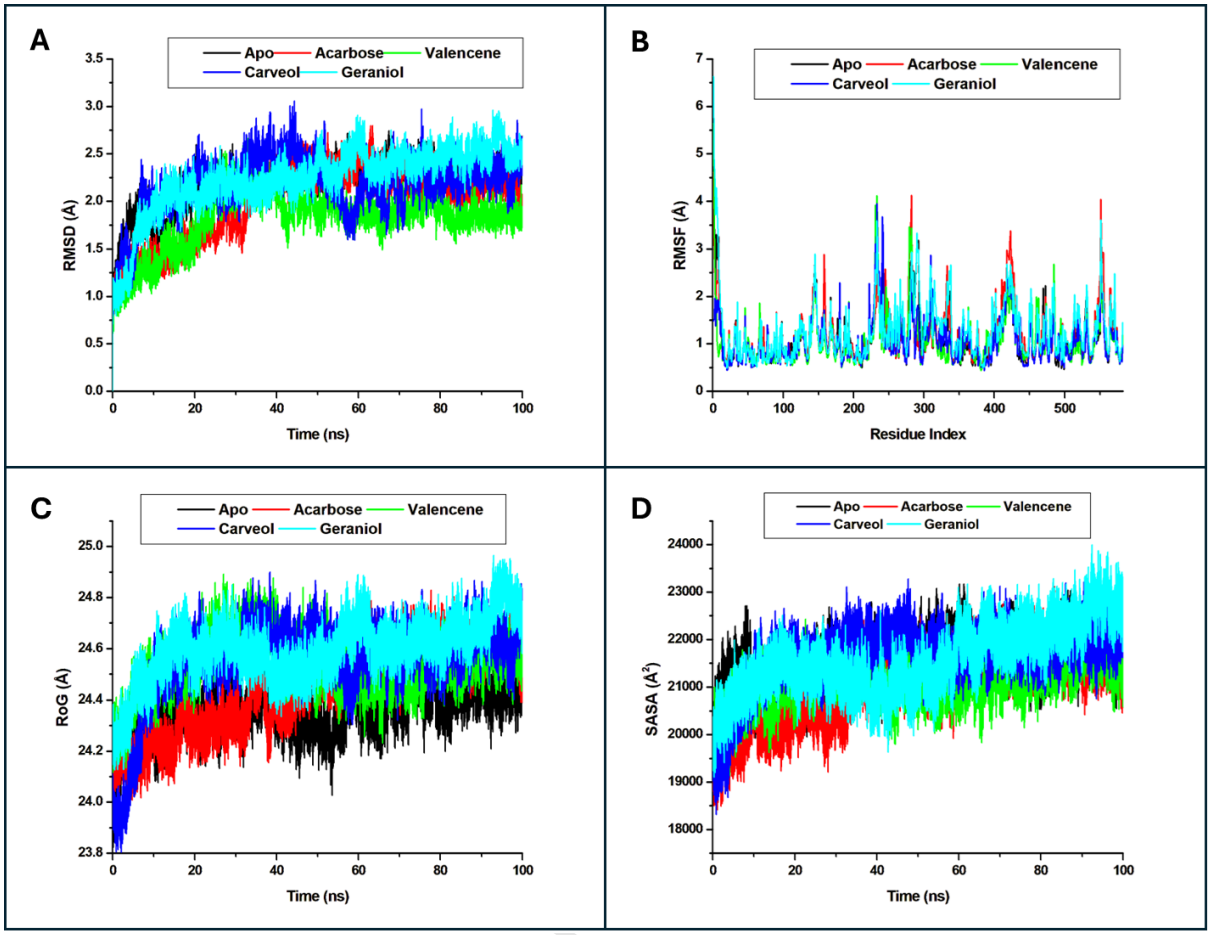

Figure 2.

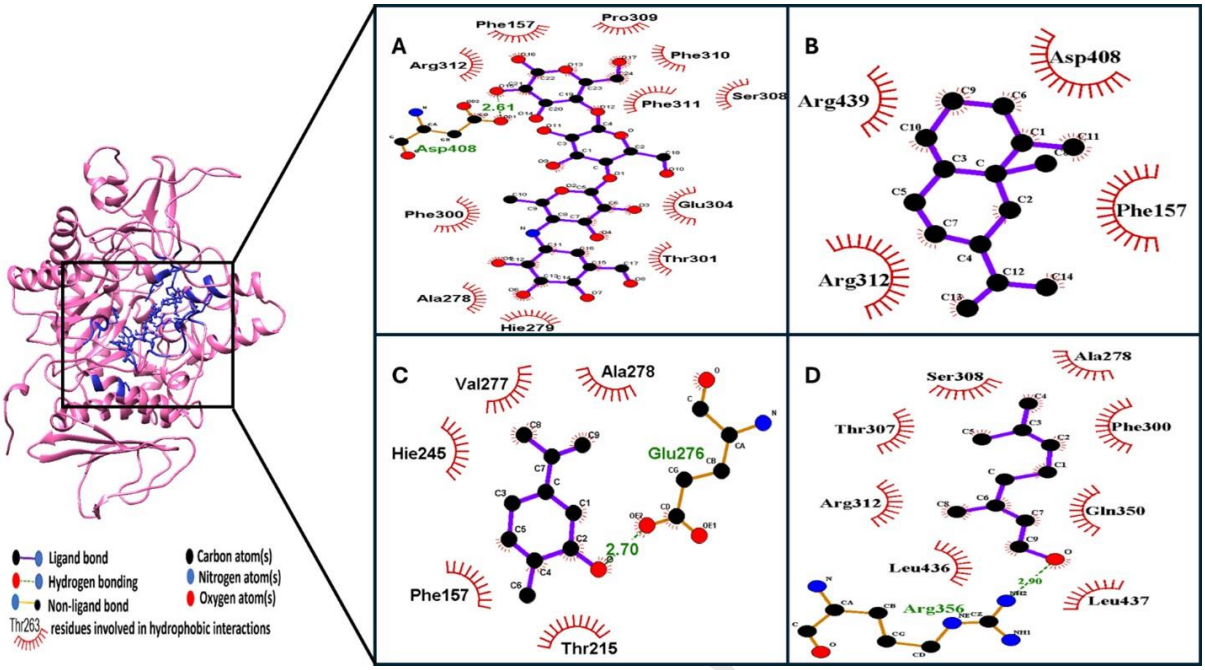

Figure 3.

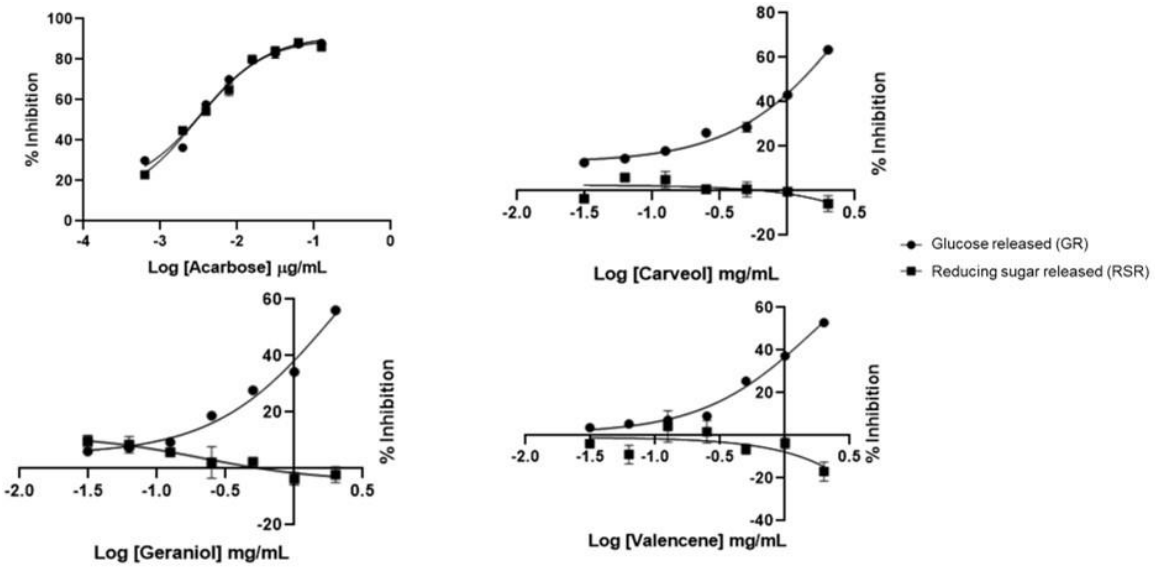

Figure 4.

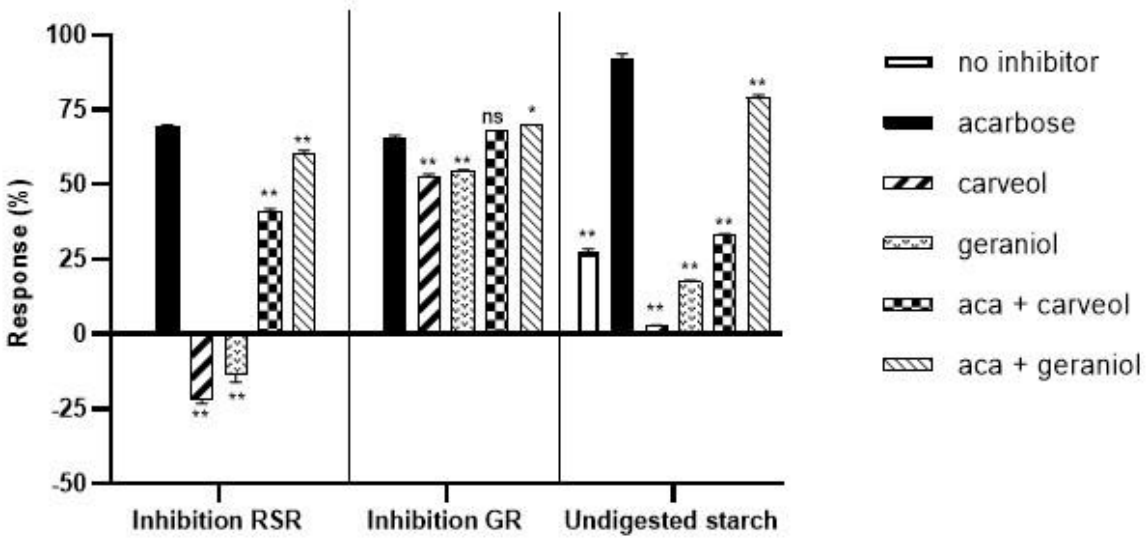

Figure 5.

Combination of Citrus peel-derived essential oils with Active Ingredient to inhibit amylolytic enzymes – a potential type II diabetes treatment approach

Highlights

- Terpenes were identified from Citrus peel-derived essential oils.
- Some individual essential oils tolerably inhibited amylolytic enzymes.
- Synergism of essential oils with Act.Ing. against amylolytic enzymes established.
- Essential oils inhibited glucose release with reduced starch residues.